

Supporting Information for

Atomic Scale Dynamics of Contact Formation in the Cross-section of InGaAs Nanowire Channels

Renjie Chen,¹ Katherine L. Jungjohann,² William M. Mook,² John Nogan,² and Shadi A. Dayeh^{1,3,4}□

¹ Department of Electrical and Computer Engineering, University of California San Diego, La Jolla, California 92093, USA

² Center for Integrated Nanotechnologies, Sandia National Laboratories, Albuquerque, New Mexico 87185, USA

³ Materials Science and Engineering Program, University of California San Diego, La Jolla, California 92093, USA

⁴ Department of NanoEngineering, University of California San Diego, La Jolla, California 92093, USA

□ email: sdayeh@ucsd.edu

Table of Contents

I. Integration of FIB lamellae onto TEM platform.....	2
II. Origin of the intermixing layer in between as-deposited Ni and InGaAs	5
III. Derivation of the diffusion model in nanowire cross-section	8
IV. In-situ TEM results for InGaAs thin-film with interfacial oxide layer	10
V. Lattice structure of nickelide phase.....	10
VI. List of supporting movies	10
References	11

I. Integration of FIB lamellae onto TEM platform

(1) Fabrication of InGaAs nanowire channels on insulator on top of Si substrate

In this work, a 50nm-thin undoped $\text{In}_{0.53}\text{Ga}_{0.47}\text{As}$ film (MBE grown on (001) InP by Intelligent Epitaxy Inc., Richardson, Texas) was first transferred on insulator on Si substrate with a solid-state wafer bonding process that we previously developed and reported elsewhere.^{1,2} After the transfer, the stacking layers from top to bottom were 50nm $\text{In}_{0.53}\text{Ga}_{0.47}\text{As}$, 15nm HfO_2 , 200nm SiO_2 , NiSi_x bonding layer (average thickness of $\sim 200\text{nm}$), and $500\mu\text{m}$ Si substrate. Secondly, the InGaAs layer was thinned down to $\sim 20\text{nm}$ with 15 cycles of digital etching that is alternative oxidation with O_2 plasma treatment (30W 3min), and oxide striping with diluted HCl solution (1:20 diluted in DI, dip for 2min). Thirdly, 20nm wide horizontal-lying nanowire structures were patterned on top of the $\text{In}_{0.53}\text{Ga}_{0.47}\text{As}$ layer utilizing a 100 kV e-beam writer (JEOL JBX-6300FS) with beam size $\sim 8\text{nm}$. Negative e-beam resist, hydrogen silsesquioxane (HSQ FOx-16), was used as the etch mask for Ar-ion milling (Intlvac) to form the $\text{In}_{0.53}\text{Ga}_{0.47}\text{As}$ nanowire channels. Ar-ion milling was chosen here instead of a chemical dry etch in order to achieve a straight nanowire sidewall. After the Ar-ion milling step, HSQ atop the nanowires was removed with three consecutive cycles of O_2 plasma treatment and a short diluted HF dip, which also reduced the etch-induced surface damage and smoothed the InGaAs surface. This resulted in a nanowire channel cross-section with a squared shape, with an edge width of $\sim 15\text{nm}$. Finally, a 100nm Ni film was deposited onto two types of nanowire samples that were prepared with different surface treatments: (i) a thin layer of $\text{In}_{0.53}\text{Ga}_{0.47}\text{As}$ surface oxide was intentionally introduced with O_2 plasma treatment (30W 3min) before Ni deposition, and (ii) the $\text{In}_{0.53}\text{Ga}_{0.47}\text{As}$ was dipped in diluted HCl solution and immediately loaded into electron-beam evaporator to prevent the formation of a native oxide layer. Type (i) specimen corresponds to the results shown in Figure 1&2 in the main text, and type (ii) specimen corresponds to the results shown in Figure 3.

To compare the interfacial properties of those two types of specimens after Ni deposition, another set of samples was prepared on a planar InGaAs film with identical interfacial treatments. As shown in Figure S1, both type (i) specimen (Fig. S1 a-c) and type (ii) specimen (Fig. S1 d-f) showed uniform interfaces over long range. With the interfacial oxide layer, the element Ni and InGaAs were separated sharply, while Ni and InGaAs were readily intermixed upon deposition at room temperature for the sample without the interfacial oxide layer. This can also be observed from elemental line-scans (Fig. S1 g-h) where the type (i) specimen had a sharp change of composition from Ni to InGaAs at the interface, and where the type (ii) specimen had a more graded change of composition from Ni to InGaAs. Inside the intermixing region, the Ni element maintained a

relatively smaller change in composition than that in the InGaAs film. This intermixing nickelide layer that is present for specimens without an interfacial oxide layer was caused by the latent heat during Ni condensation from vapor phase into solid phase as will be further discussed in section II.

(2) Specimen lamellae preparation by focused-ion-beam (FIB) milling and in-situ lift-out (ILO)

TEM specimens in this work were prepared by FIB milling on the samples of InGaAs nanowire on insulator on Si substrate. Prior to FIB milling, 400nm SiO₂ and 50nm Pt were deposited atop the sample to prevent damage of interested area under ion beams. SiO₂ layer here was deposited at a low temperature (100 °C) plasma enhanced chemical vapor deposition (PECVD) process to prevent any possible reaction between Ni contact and InGaAs nanowires. The FIB and INLO process utilized here, shown in Figure S2 first row, follow conventional procedures,^{3,4} in which a 30 kV Ga beam was used for rough milling and reduced voltage and current (10 kV, 0.1 nA) was used for fine milling.

(3) Transferring specimen lamellae on top of thermal E-chips

The process to transfer FIB lamellae onto the TEM window of a thermal E-chip (AHA chip, Protochips Inc.) was shown in Figure S2, second row. The TEM window was made of conductive ceramic with many manmade circular holes for e-beam transparency. We intentionally drilled a larger rectangular hold for better imaging of our FIB lamellae for the HRTEM video recording of the reaction dynamics. We also deposited two 3 μm tall Pt posts on the edge of the opening region (shown in Fig. S2 step 5) to hold the transferred FIB lamellae. These two Pt posts not only helped maintaining the flatness of specimen lamellae during transfer, but also facilitated further thinning and cleaning steps by lifting up the lamellae from the surface of ceramic membrane. Finally, the transferred specimen lamellae was further thinned with FIB with reduced voltage and current (10 kV, 0.1 nA), until the lamellae reached a thickness ~ 60nm.

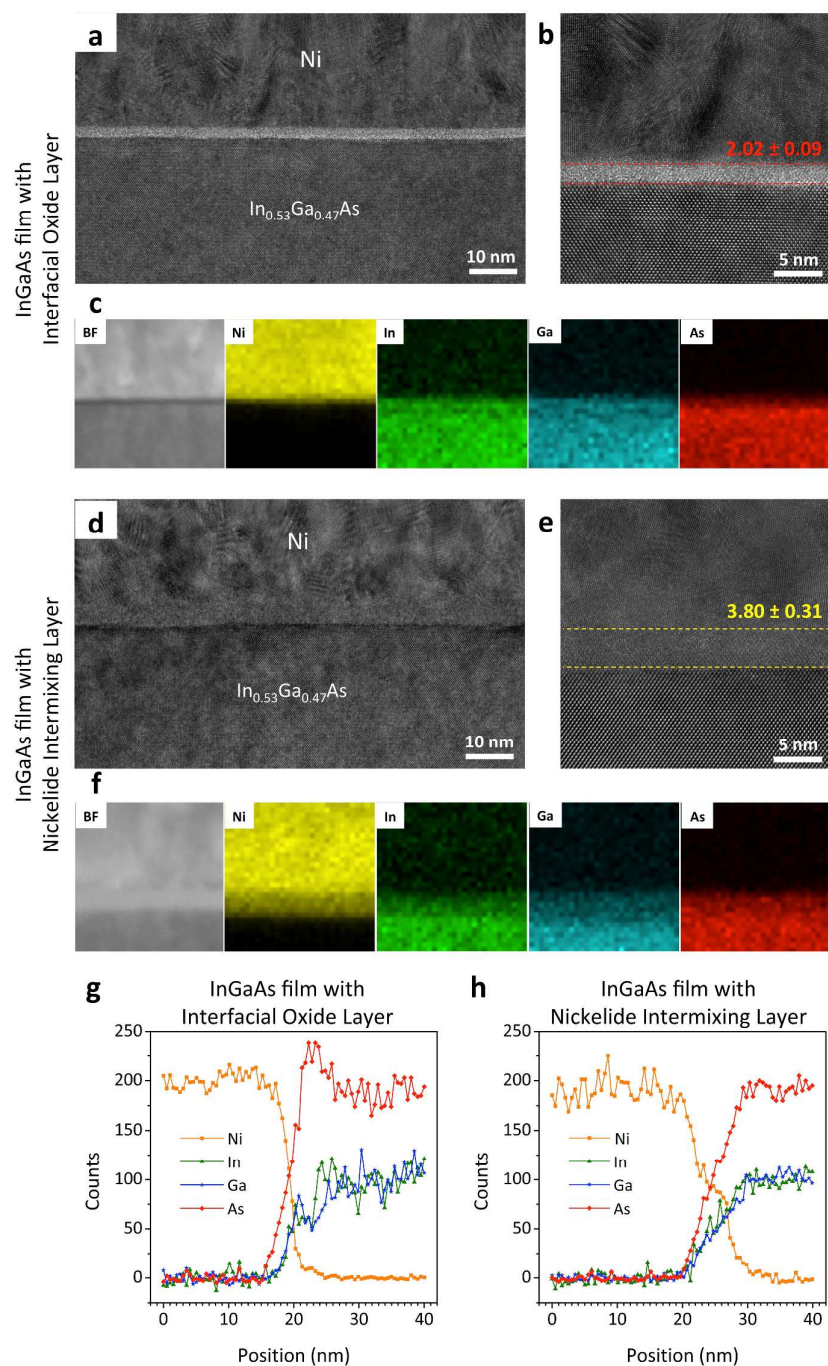


Figure S1 | Comparison of interfacial structures for two types of specimens on InGaAs thin film. **a-c**, TEM, HRTEM, and EDS mapping of type (i) specimen at the interface between Ni and InGaAs film. The light contrast layer at the interface, i.e. InGaAs surface oxide layer, has a uniform thickness of 2.02 ± 0.09 nm. The EDS mapping of four elements show the sharp interface between Ni and InGaAs, indicating that the interfacial oxide layer effectively prevents the intermixing of Ni and InGaAs. **d-f**, TEM, HRTEM, and EDS mapping of type (ii) specimen at the interface between Ni and InGaAs film. The amorphous layer at the interface, i.e. Ni and InGaAs intermixing layer, has a uniform thickness of 3.80 ± 0.31 nm. The EDS mapping of four elements show the clear evidence of intermixing between Ni and InGaAs at the interface. **g-h**, the EDS line-scan across the interface of type (i) and type (ii) specimens, respectively. Ni and As elemental counts are normalized according to their averaged top flats.

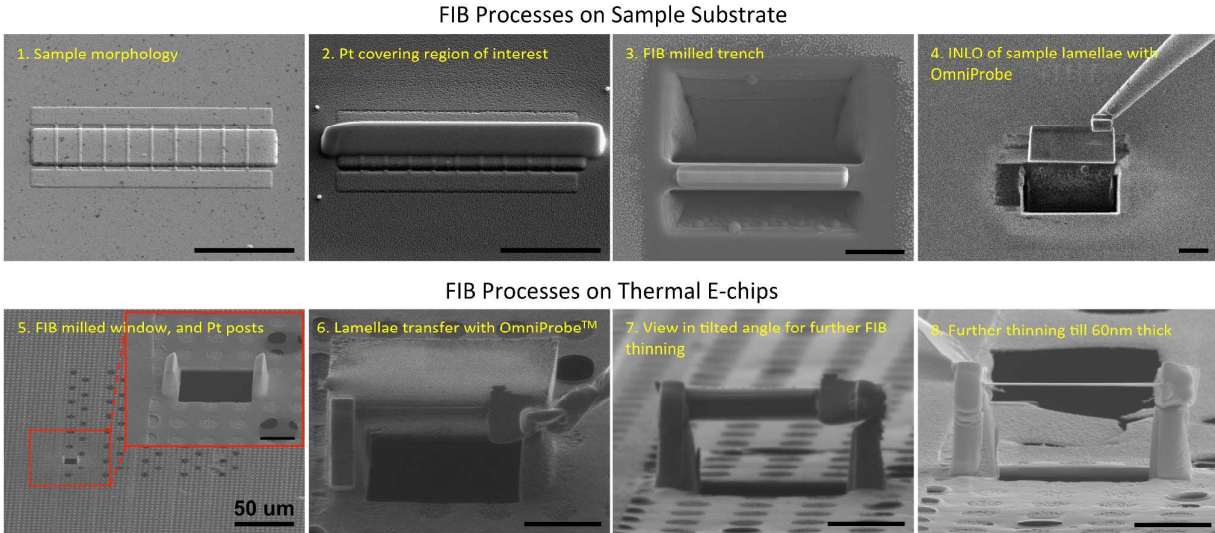


Figure S2 | Sequences in FIB processes. SEM images show the fabrication sequences to transfer the FIB cut lamellae from the home substrate onto the TEM membrane window of a thermal E-chipTM. All the scale bars are 5 μ m, except the one labeled separately in step 5.

II. Origin of the intermixing layer in between as-deposited Ni and InGaAs

There are several possible reasons that may cause the intermixing between as-deposited Ni and InGaAs, including chamber overheating during evaporation, ion-beam-induced metal-semiconductor reaction,^{5,6} or latent heat released from the condensation of metal atoms from vapor phase,^{7,8} which we validated to be the cause below.

Firstly, we deposited the Ni in our experiments with an electron-beam evaporator with a total thickness of 100nm. Ni was deposited slowly (0.7 $\text{\AA}/\text{s}$) to prevent exaggerated stress and overheating, and the chamber was cooled down for 30min halfway after the deposition of the first 50nm of Ni. We also did a control experiment by depositing Ni by sputtering at room temperature where the surface pre-deposition treatments for InGaAs were similar to those samples that underwent electron-beam evaporation. The results are shown in Figure S3, with very similar interfacial structures as those with e-beam evaporated Ni, indicating that the Ni-InGaAs intermixing layer was not introduced by over-heating in the electron-beam evaporation chamber.

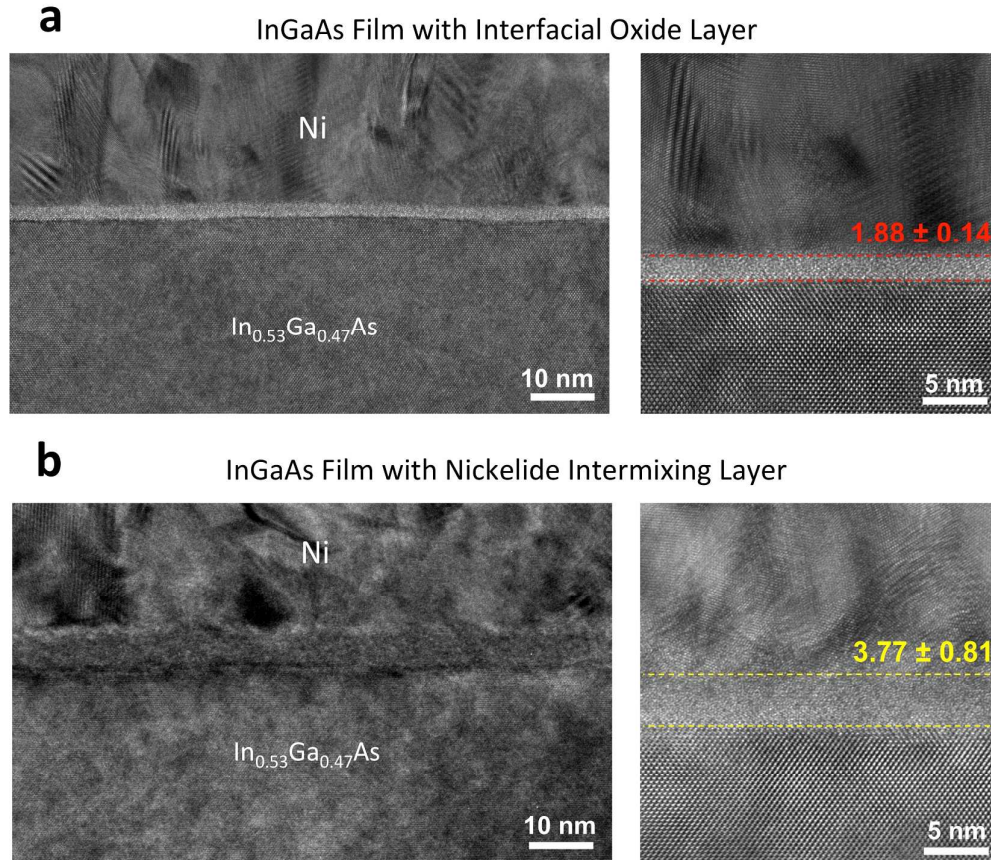


Figure S3 | Comparison of interfacial structures when Ni deposited by sputtering. **a**, TEM and HRTEM images of type (i) specimen at the interface between Ni and InGaAs film. The light contrast layer at the interface, i.e. InGaAs surface oxide layer, has a uniform thickness of 1.88 ± 0.14 nm. **b**, TEM and HRTEM images of type (ii) specimen at the interface between Ni and InGaAs film. The amorphous layer at the interface, i.e. Ni and InGaAs intermixing layer, has a nearly uniform thickness of 3.77 ± 0.81 nm.

Similarly, we excluded the possibility of ion-beam-induced metal-semiconductor reaction, also called ion-beam mixing, by processing FIB milling in a tilted angle (shown in Figure S4). Here, the Ni layer was deposited on two ends of InGaAs channel with HCl treated surface (no surface oxides present). After FIB milling, the interface structures were characterized under TEM. We found that the Ni-InGaAs intermixing layers were identical on both sides, and that both of them extended slightly out of the edge of Ni contacts. Ion-beam mixing is usually caused by penetrating energetic ions through the interface between a metal-film and semiconductor, overcoming equilibrium constraints in localized regions, and forcing atomic rearrangement, which will be localized and directional. This is contradictory to our observations here.

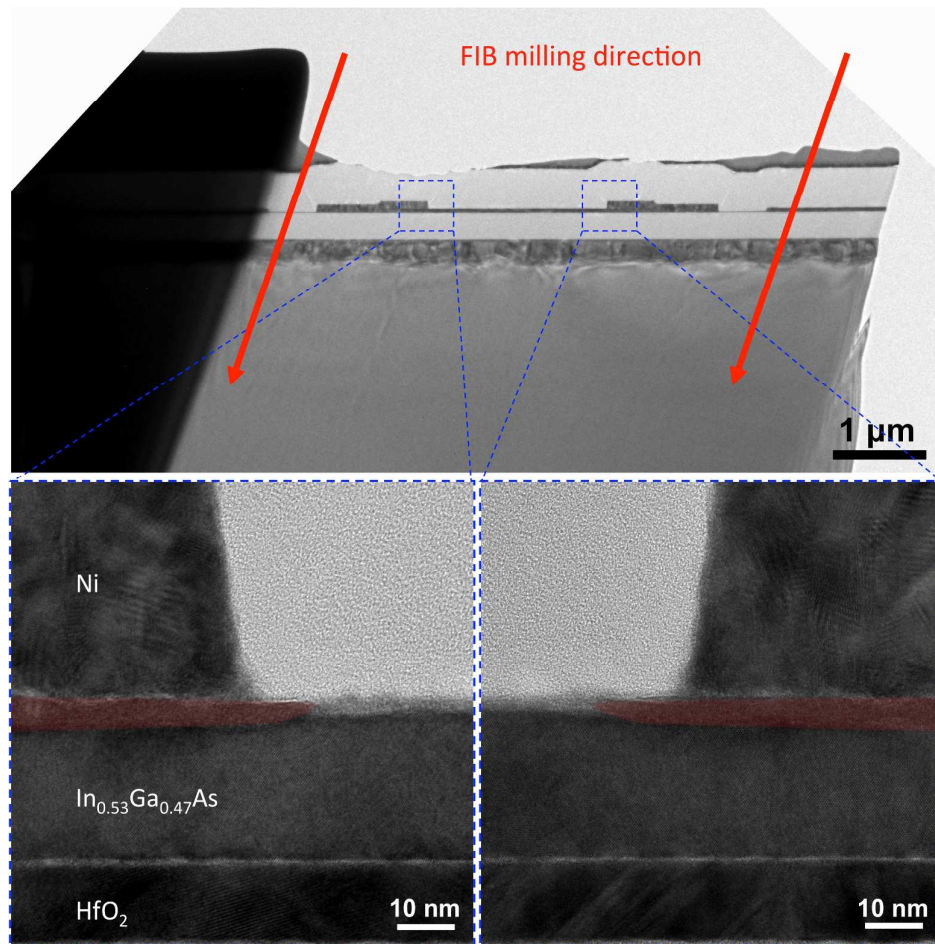


Figure S4 | Interfacial structures when specimen is milled by FIB in a tilted angle. TEM images of a type (ii) specimen in which Ni contacts were deposited at two ends of the InGaAs channel. The specimen was milled by FIB in a tilted angle in the direction of the red arrows in the top panel. Zoomed in TEM images show identical Ni-InGaAs intermixing layers on both sides, and both intermixing layers extended slightly out of the edge of Ni contacts. The evolution of the nickelide extended region to the right from the left contact indicates that the Ni-InGaAs intermixing is not introduced by the directional ion-beam induced mixing (directed to the left of the sample).

The third possibility is that the latent heat released from the condensation of metal atoms from vapor phase. In fact, when a metal and a semiconductor are brought in contact at room temperature, an intermixing layer can be readily formed between them due to the screening coulomb interaction by free electrons in the metal, which weakens the covalent bonding energy at the semiconductor surface.^{9,10} However, the intermixing layer due to electron screening is usually a monolayer or two thick. It has been previously observed that the as-deposited metal on semiconductor can introduce thicker (few nanometers) amorphous intermixture caused by the negative heat (latent heat) from metal condensation. The amorphous interfacial layers between the deposited metal and semiconductor were also observed in other metal/III-V systems.^{11,12}

III. Derivation of the diffusion model in nanowire cross-section

The fluxes of Ni atoms in the three processes as shown in Figure 4, can be expressed as:

$$F_1 = k_{dissolve} (C_{Ni/Nickelide}^{eq} - C_R) \cdot 2\pi R h = k_{dissolve} (C_{Ni/Nickelide}^{eq} - C_R) \cdot hL \quad (S3.1)$$

$$F_2 = D_{Ni} (C_r - C_R) \cdot 2\pi h \cdot \left[\ln\left(\frac{r(t)}{R}\right) \right]^{-1} = D_{Ni} (C_r - C_R) \cdot 2\pi h \cdot \left[\ln\left(\frac{l(t)}{L}\right) \right]^{-1} \quad (S3.2)$$

$$F_3 = k_{growth} (C_r - C_{Nickelide/InGaAs}^{eq}) \cdot 2\pi r(t) h = k_{growth} (C_r - C_{Nickelide/InGaAs}^{eq}) \cdot hl(t) \quad (S3.3)$$

where $k_{dissolve}$ and k_{growth} are the rate constants for Ni dissolution and nickelide growth respectively.

$C_{Ni/Nickelide}^{eq}$ and C_R represents the equilibrium and instant Ni concentrations across the Ni/nickelide interface. C_r and $C_{Nickelide/InGaAs}^{eq}$ denotes the instant and equilibrium Ni concentrations across the nickelide/In_{0.53}Ga_{0.47}As interface.

Derivation of equation F₂:

Considering Fick's first law of diffusion in cylindrical coordinates, we can write:

$$\vec{J} = -D \frac{dC}{dr} \vec{r}.$$

The Ni atomic flux can be expressed as $F = D \frac{dC}{dr} \cdot 2\pi r h$, pointing to the core.

Integration of the equation $\frac{F}{2\pi r h \cdot D} dr = dC$ across the entire nickelide region yields:

$$\int_R^r \frac{F}{2\pi r h \cdot D} dr = \int_{C_R}^{C_r} dC$$

Therefore, we can write:

$$\frac{F}{2\pi h \cdot D} \ln\left(\frac{r}{R}\right) = C_r - C_R, \Rightarrow F = D(C_r - C_R) \cdot 2\pi h \cdot \left[\ln\left(\frac{r}{R}\right) \right]^{-1}$$

Under steady state condition, $F_1=F_2=F_3=F$, we can obtain a characteristic equation of the reaction as follows:

$$F = k_{dissolve} (C_{Ni/Nickelide}^{eq} - C_R) \cdot hL = D_{Ni} (C_r - C_R) \cdot 2\pi h \cdot \left[\ln\left(\frac{l(t)}{L}\right) \right]^{-1} = k_{growth} (C_r - C_{Nickelide/InGaAs}^{eq}) \cdot hl(t), \quad (S3.4)$$

hence:

$$F = \frac{C_{Ni/Nickelide}^{eq} - C_{Nickelide/InGaAs}^{eq}}{\frac{1}{k_{dissolve} \cdot hL} - \frac{\ln\left(\frac{l(t)}{L}\right)}{D_{Ni} \cdot 2\pi h} + \frac{1}{k_{growth} \cdot hl(t)}}. \quad (S3.5)$$

Because of mass conservation, $F \cdot \frac{M_{\text{Nickelide}}}{N_A \cdot \rho_{\text{Nickelide}}} = -2\pi r(t)h \cdot \frac{dr(t)}{dt} = -\frac{hl(t)}{2\pi} \cdot \frac{dl(t)}{dt}$ (S3.6)

and assuming that $P = \frac{2\pi M_{\text{Nickelide}}}{N_A \cdot \rho_{\text{Nickelide}}} \cdot (C_{\text{Ni/Nickelide}}^{\text{eq}} - C_{\text{Nickelide/InGaAs}}^{\text{eq}})$ (S3.7)

we can write,

$$\frac{dl(t)}{dt} = -\frac{P}{\frac{l(t)}{k_{\text{dissolve}}L} - \frac{l(t) \cdot \ln\left(\frac{l(t)}{L}\right)}{2\pi D_{\text{Ni}}} + \frac{1}{k_{\text{growth}}}} \quad (\text{S3.8})$$

Here, the three terms in the denominator represent three rate-limiting mechanisms. If these three rate-limiting mechanisms are separately considered, the differential equation can be solved.

(i) If Ni dissolution at the Ni/nickelide interface is the rate-limiting step, we obtain:

$$\frac{dl(t)}{dt} \approx -\frac{P \cdot k_{\text{dissolve}}L}{l(t)}, \quad \text{therefore: } l(t) = \sqrt{L^2 - 2k_{\text{dissolve}}LP \cdot t}. \quad (\text{S3.9})$$

(ii) If nickelide growth at the nickelide/InGaAs interface is the rate-limiting step, we obtain:

$$\frac{dl(t)}{dt} \approx -P \cdot k_{\text{growth}}, \quad \text{therefore: } l(t) = L - k_{\text{growth}}P \cdot t. \quad (\text{S3.10})$$

(iii) If the Ni diffusion in the reacted nickelide region is the rate-limiting step, we obtain:

$$\frac{dl(t)}{dt} \approx P \cdot \frac{2\pi D_{\text{Ni}}}{l(t) \cdot \ln\left(\frac{l(t)}{L}\right)}, \quad \text{therefore: } 2l(t)^2 \ln\left(\frac{l(t)}{L}\right) + L^2 - l(t)^2 = 8\pi D_{\text{Ni}}P \cdot t. \quad (\text{S3.11})$$

Solution of the Differential equation S3.11:

To solve the equation $l(t) \cdot \ln\left(\frac{l(t)}{L}\right) dl(t) = 2\pi D_{\text{Ni}}P dt$,

we can assume $y = \frac{l(t)}{L}$, and then obtain $L^2 y \ln y dy = 2\pi D_{\text{Ni}}P dt$.

We then perform integration of this equation across the entire nickelide region:

$$\int_1^{l(t)/L} L^2 y \ln y dy = \int_0^t 2\pi D_{\text{Ni}}P dt$$

Using known integrals for logarithmic functions, $\int x \ln x dx = x^2 \left(\frac{\ln x}{2} - \frac{1}{4} \right)$, we obtain:

$$L^2 y^2 \left(\frac{\ln y}{2} - \frac{1}{4} \right) \Big|_1^{l(t)/L} = 2\pi D_{\text{Ni}}P \cdot t, \Rightarrow 2l(t)^2 \ln\left(\frac{l(t)}{L}\right) + L^2 - l(t)^2 = 8\pi D_{\text{Ni}}P \cdot t. \text{ We utilize this}$$

equation in the fits of Fig. 4c of the main text.

IV. In-situ TEM results for InGaAs thin-film with interfacial oxide layer

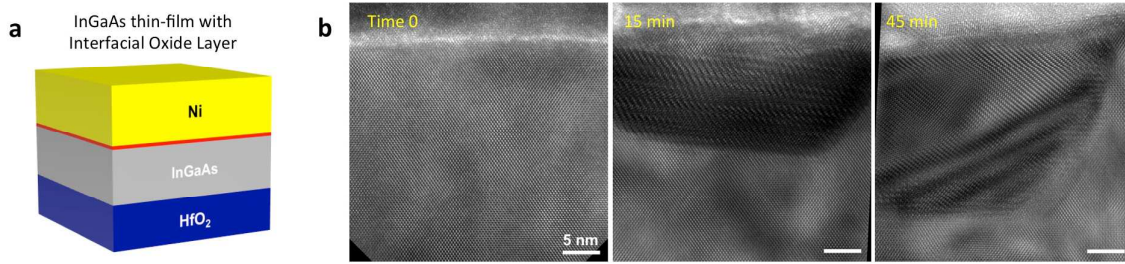


Figure S5 | In-situ heating TEM results for $\text{In}_{0.53}\text{Ga}_{0.47}\text{As}$ thin film sample. **a**, schematic image shows the stacking of Ni on planar InGaAs film with a thin InGaAs oxide layer at the interface. **b**, the time sequenced HRTEM images of the in-situ heating experiment performed at 290 °C. At time 0, the Ni contact was separated from InGaAs by the surface oxide layer. Then, Ni gradually diffused into InGaAs and formed crystalline nickelide phase without transitioning through an amorphization step. In the first 15min, the nickelide structure was polycrystalline with overlapped grains forming moiré pattern. Beyond 15min and up to the end of recording time of 45min, the slightly misaligned polycrystalline nickelide gradually transferred into single crystalline structure directly under the nickel contact.

V. Lattice structure of nickelide phase

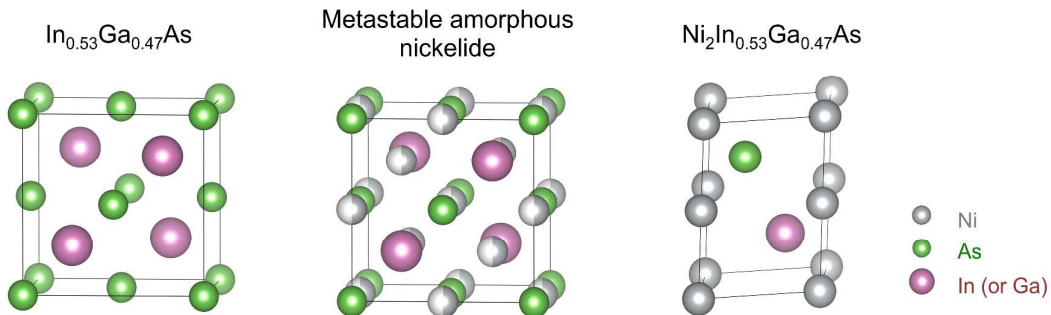


Figure S6 | Lattice structures of pristine $\text{In}_{0.53}\text{Ga}_{0.47}\text{As}$, metastable amorphous nickelide phase, and crystalline $\text{Ni}_2\text{In}_{0.53}\text{Ga}_{0.47}\text{As}$ phase. Non-reacted $\text{In}_{0.53}\text{Ga}_{0.47}\text{As}$ has the zinc-blende structure with lattice constant of $a = 5.87 \text{ \AA}$. During the amorphization step, we hypothesize that Ni diffused into the tetrahedral interstitial sites of the $\text{In}_{0.53}\text{Ga}_{0.47}\text{As}$ lattice, occupied part of them and formed a metastable nickelide phase. The crystalline $\text{Ni}_2\text{In}_{0.53}\text{Ga}_{0.47}\text{As}$ lattice is hexagonal and adopts the NiAs (B8) structure with lattice constants of $a = 3.93 \text{ \AA}$, $c = 5.10 \text{ \AA}$.²

VI. List of supporting movies

Movie S1: Solid-state amorphization process during Ni reaction with InGaAs nanowire cross-section that had a thin InGaAs surface oxide layer in between. The reaction was recorded

at 180 °C. The frame rate is accelerated by 8 times.

Movie S2: Solid-state amorphization process during Ni reaction with InGaAs nanowire cross-section that had a Ni-InGaAs intermixing layer in between before the reaction started. The reaction was recoded at 180 °C. The frame rate is accelerated by 8 times.

Movie S2: Solid-state regrowth of the amorphous nickelide phase into well-aligned crystalline structure. The reaction was recoded at 375 °C. The frame rate is accelerated by 8 times. Scale bars in all movies are 2 nm.

References

- 1 Dai, X., Nguyen, B. M., Hwang, Y., Soci, C. & Dayeh, S. A. Novel heterogeneous integration technology of III–V layers and InGaAs finFETs to silicon. *Advanced Functional Materials* **24**, 4420-4426 (2014).
- 2 Chen, R. & Dayeh, S. A. Size and Orientation Effects on the Kinetics and Structure of Nickelide Contacts to InGaAs Fin Structures. *Nano letters* **15**, 3770-3779 (2015).
- 3 Giannuzzi, L. A. *et al.* in *Introduction to focused ion beams* 201-228 (Springer, 2005).
- 4 Mayer, J., Giannuzzi, L. A., Kamino, T. & Michael, J. TEM sample preparation and FIB-induced damage. *Mrs Bulletin* **32**, 400-407 (2007).
- 5 Lau, S. *et al.* Ion-beam mixing of metal-semiconductor eutectic systems. *Nuclear Instruments and Methods* **182**, 97-105 (1981).
- 6 Nastasi, M. & Mayer, J. Ion beam mixing in metallic and semiconductor materials. *Materials Science and Engineering: R: Reports* **12**, 1-52 (1994).
- 7 Sands, T. *et al.* Ni, Pd, and Pt on GaAs: A comparative study of interfacial structures, compositions, and reacted film morphologies. *Journal of Materials Research* **2**, 262-275 (1987).
- 8 Ko, D. H. & Sinclair, R. Amorphous phase formation and initial interfacial reactions in the platinum/GaAs system. *Journal of applied physics* **72**, 2036-2042 (1992).
- 9 Hiraki, A., Shuto, K., Kim, S., Kammura, W. & Iwami, M. Room - temperature interfacial reaction in Au - semiconductor systems. *Applied Physics Letters* **31**, 611-612 (1977).
- 10 Hiraki, A. A Model on the Mechanism of Room Temperature Interfacial Intermixing Reaction in Various Metal - Semiconductor Couples: What Triggers the Reaction? *Journal of The Electrochemical Society* **127**, 2662-2665 (1980).
- 11 Sands, T., Keramidias, V., Washburn, J. & Gronsky, R. Structure and composition of NixGaAs. *Applied physics letters* **48**, 402-404 (1986).
- 12 Ko, D. H. & Sinclair, R. Amorphous phase formation in an as - deposited platinum - GaAs interface. *Applied physics letters* **58**, 1851-1853 (1991).